

## Data assimilation Experiments using the Diffusive Back and Forth Nudging for the NEMO ocean model

Ruggiero, G. A.<sup>1</sup>, Ourmières, Y.<sup>2</sup>, Cosme, E.<sup>3</sup>, Blum, J.<sup>1</sup>, Auroux, D.<sup>1</sup>, and Verron, J.<sup>4</sup>

<sup>1</sup>Université de Nice Sophia-Antipolis/LJAD, Nice, France

<sup>2</sup> Université du Sud Toulon-Var, Aix-Marseille Université, CNRS/INSU, IRD, Mediterranean Institute of Oceanography (MIO), France

<sup>3</sup>Université Joseph Fourier/LGGE, Grenoble, France

<sup>4</sup>CNRS/LGGE, Grenoble, France

*Correspondence to:* Giovanni A. Ruggiero  
giovanni.ruggiero@unice.fr

1 **Abstract.** The Diffusive Back and Forth Nudging (DBFN) is an easy-to-implement iterative data  
2 assimilation method based on the well-known Nudging method. It consists in a sequence of forward  
3 and backward model integrations, within a given time window, both of them using a feedback term  
4 to the observations. Therefore in the DBFN, the Nudging asymptotic behavior is translated into an  
5 infinite number of iterations within a bounded time domain. In this method, the backward integra-  
6 tion is carried out thanks to what is called backward model, which is basically the forward model  
7 with reversed time step sign. To maintain numeral stability the diffusion terms also have their sign  
8 reversed, giving a diffusive character to the algorithm. In this article the DBFN performance to con-  
9 trol a primitive equation ocean model is investigated. In this kind of model non-resolved scales are  
10 modeled by diffusion operators which dissipate energy that cascade from large to small scales. Thus,  
11 in this article the DBFN approximations and their consequences on the data assimilation system set-  
12 up are analyzed. Our main result is that the DBFN may provide results which are comparable to  
13 those produced by a 4Dvar implementation with a much simpler implementation and a shorter CPU  
14 time for convergence. The conducted sensitivity tests show that the 4Dvar profits of long assimi-  
15 lation windows to propagate surface information downwards, and that for the DBFN, it is worth using  
16 short assimilation windows to reduce the impact of diffusion-induced errors.

17 **Keywords.** Data Assimilation, Nudging, Back and Forth Nudging, NEMO

## 18 1 Introduction

19 The well-known Nudging method is based on the second Newton axiom and consists in adding a  
20 forcing term in the right hand side of a given system in order to gently push the model toward a  
21 prescribed value. The first appearance of nudging in the geophysical literature was in 1974 (Anthes,  
22 1974). In this work the authors proposed the use of nudging to mitigate initialization problems in at-  
23 mospheric models. However, a similar algorithm had already been developed by Luenberger (1966).  
24 This algorithm has been called "Luenberger observer" or "asymptotic estimator", since under lin-  
25 earity and observability hypothesis the estimator error converges to zero for time tending to infinity.  
26 It is quite interesting to note that there is no mention of the Luenberger observer in the geophysical  
27 literature except in the recent work of Auroux and Blum (2005). More recently, a comprehensive  
28 study on the nudging method and its variants was produced by Blum et al. (2008) and Lakshmivara-  
29 han and Lewis (2012).

30 The first appearance of a successful application of nudging to ocean Data Assimilation (DA) was  
31 in 1992 in a work that assimilated sea surface height derived from satellite measurements into a  
32 quasi-geostrophic layered model (Verron, 1992). Since then, the method has been successfully ap-  
33 plied to several oceanographic numerical problems such as the estimation of boundary conditions  
34 (Marchesiello et al., 2001; Chen et al., 2013), downscaling (Li et al., 2012), and other DA problems  
35 (Verron, 1992; Haines et al., 1993; Blayo et al., 1994; Lewis et al., 1998; Killworth et al., 2001;  
36 Thompson et al., 2006). Concerning applications to DA problems, the weights given to the model  
37 and the observations are generally not based on any optimality condition, but are rather scalars or  
38 Gaussian-like functions constructed based on physical assumptions or empirical considerations. The  
39 appeals of this method are the simplicity of implementation in complex numerical models, the low  
40 computational power required and the time smoothness of the solution.

41 The increasing availability of computing power has allowed to use more advanced data assimi-  
42 lation methods. In general, these methods use information on the model statistics and observations  
43 errors to weight the model-observations combination. Two of these methods that are widely used by  
44 prediction centers are the ensemble Kalman filter- EnKF (Evensen, 1994) and its variations (Pham,  
45 2001; Hunt et al., 2007), and the four dimensional variational method 4Dvar (Le Dimet and Tala-  
46 grand, 1986; Courtier et al., 1994). For the first, the numerical costs are due to the propagation of the  
47 ensemble, usually formed by tenths of members, to calculate the forecast. For the second, the costs  
48 are due to the need of minimizing a cost function in a very large state space ( $10^8$  variables). This  
49 requires several iterations of the minimization algorithm, which involves several integrations of the  
50 direct and adjoint models.

51 However, even with the growing interest in these complex techniques built on solid theoretical  
52 arguments, nudging has not been left aside. Recent works have used nudging along with more  
53 advanced methods such as Optimal interpolation (Clifford et al., 1997; Wang et al., 2013), EnKF  
54 (Ballabrera-Poy et al., 2009; Bergemann and Reich, 2010; Lei et al., 2012; Luo and Hoteit, 2012),



55 4Dvar (Zou et al., 1992; Stauffer and Bao, 1993; Vidard et al., 2003; Abarbanel et al., 2010) or  
56 particle filters (Luo and Hoteit, 2013; Lingala et al., 2013) to extract the best of each method. In  
57 the particular case of the hybridization with the EnKF proposed by Lei et al. (2012), the resulting  
58 algorithm takes the advantage of the dynamical propagation of the covariance matrix from the EnKF  
59 and uses nudging to mitigate problems related to the intermittence of the sequential approach, which  
60 among other things entails the possible discarding of some observations.

61 Recently, Aurox and Blum (2005) revisited the nudging method and proposed a new observer  
62 called Back and Forth Nudging (BFN). The BFN consists in a sequence of forward and backward  
63 model integrations, both of them using a feedback term to the observations, as in the direct nudg-  
64 ing. The BFN integrates the direct model backwards in time avoiding the construction of the adjoint  
65 and/or tangent linear models needed by 4DVar. Therefore, it uses only the fully non-linear model to  
66 propagate information forward and backward in time. The nudging gain, which has an opposite sign  
67 with respect to the forward case, has a double role: push the model toward observations and stabilize  
68 the backward integration, which is especially important when the model is not reversible.

69 The BFN convergence was proved by Aurox and Blum (2005) for linear systems of ordinary  
70 differential equations and full observations, by Ramdani et al. (2010) for reversible linear partial dif-  
71 ferential equations (Wave and Schrödinger equations), by Donovan et al. (2010) and Leghtas et al.  
72 (2011) for the reconstruction of quantum states and was studied by Aurox and Nodet (2012) for  
73 non-linear transport equations. The BFN performance in numerical applications using a variety of  
74 models, including non-reversible models such as a Shallow Water (SW) model (Aurox, 2009) and  
75 a Multi-Layer Quasi-Geostrophic (LQG) model (Aurox and Blum, 2008), are very encouraging.  
76 Moreover, by using a simple scalar gain, it produced results comparable to those obtained with  
77 4DVar but with lower computational requirements (Aurox, 2009; Aurox et al., 2012).

78 In this article we present for the first time a BFN application to control a primitive equation  
79 ocean model. The numerical model used is NEMO (Madec, 2008), currently used by the French op-  
80 erational center, Mercator Océan (<http://www.mercator-ocean.fr/fre>), to produce and deliver ocean  
81 forecasts. The well-known idealized double gyre configuration at eddy-permitting resolution is used.  
82 This configuration has the advantage of being simple from the geometry and forcings point of view  
83 at the same time it reproduces most of features found in a middle latitude ocean basin.

84 The BFN application to control a primitive equation ocean model represents a new challenge  
85 due to the increased model complexity. Among the differences between NEMO and the simplified  
86 oceanic models used by Aurox and Blum (2008) and Aurox (2009) stand out the more complex  
87 relationship between the variables in the former since no filtering technique is used in the derivation  
88 of the physical model (except the Boussinesq approximation which is also considered by the SW  
89 and LQG models), and the inclusion of an equation for the conservation of the thermodynamical  
90 properties. The latter requires the use of a nonlinear state equation to couple dynamical and thermo-  
91 dynamical variables.

92 Furthermore, the vertical ocean structure represented by NEMO is more complex than the verti-  
 93 cal ocean structure represented by the SW and LQG used by Auroux and Blum (2008) and Auroux  
 94 (2009). This is because the SW model has no vertical levels and the LQG was implemented with  
 95 only 3 layers, while in this article NEMO is configured with 11 vertical layers. In addition, NEMO  
 96 considers vertical diffusion processes, mostly ignored by the LQG model. Vertical diffusion plays an  
 97 important role in maintaining the ocean stratification and meridional overturning circulation, which  
 98 is directly related to the transport of heat in the ocean. Moreover from the practical point of view,  
 99 the diffusion/viscosity required to keep the NEMO simulations stable is by far greater than for the  
 100 SW or LQG at the same resolution.

101 These issues call into question the validity of the approximations made by the BFN under realistic  
 102 conditions. Thus, our primary objective is to study the possibility of applying the BFN in realistic  
 103 models and evaluate its performance compared to the 4Dvar. This appears as being the next logical  
 104 step before using the BFN to assimilate real data.

105 This article is organized as follows. In Sect 2 the BFN and the 4Dvar are described. Section 3  
 106 describes the model physics and the model set-up. Section 4 discusses some practical aspects of  
 107 the backwards integration. Section 5 presents the BFN and the 4Dvar set-up and the designed data  
 108 assimilation experiments. Finally, the data assimilation results are presented in the Sect 6, on which  
 109 we discuss the impact of the length of the data assimilation window on the method performances.

## 110 2 Data Assimilation Methods

111 In this section the Back and Forth Nudging (BFN) is introduced and the 4Dvar used to assess the  
 112 BFN performance is briefly described.

### 113 2.1 The Back and Forth Nudging

114 The conventional nudging algorithm consists in adding a forcing term (feedback term) to the model  
 115 equations, proportional to the difference between the data and the model at a given time. More  
 116 generally, given a model described by a set of ordinary equations (or discretized partial differential  
 117 equations), nudging consists in adding to them the forcing term  $\mathbf{K}(\mathbf{x}_{obs} - \mathcal{H}(\mathbf{x}))$ :

$$118 \frac{d\mathbf{x}}{dt} = \mathcal{F}(\mathbf{x}) + \mathbf{K}(\mathbf{x}_{obs} - \mathcal{H}(\mathbf{x})) \quad (1)$$

119 where  $\mathbf{x}$  represents the state vector,  $\mathcal{F}$  is the model operator,  $\mathcal{H}$  is the observation operator allow-  
 120 ing one to compare the observations  $\mathbf{x}_{obs}(t)$  to the corresponding system state  $\mathcal{H}(\mathbf{x})$ , and  $\mathbf{K}$  is the  
 121 nudging gain matrix. In this algorithm the model appears as a weak constraint. The feedback term  
 122 changes the dynamical equations and forces the state variables to fit the observations as well as pos-  
 123 sible.

124 In the linear case, i.e. when  $\mathcal{F}$  and  $\mathcal{H}$  may be written as matrices  $\mathbf{F}$  and  $\mathbf{H}$ , and in the absence  
 125 of noise in the system, nudging is nothing else than the Luenberger observer (Luenberger, 1966). In

126 this case, and assuming that the observability of the pair  $(\mathbf{F}, \mathbf{H})$  holds, there is a class of possible  
 127 values of  $\mathbf{K}$  that guarantees the estimator convergence when  $t \rightarrow \infty$  (Gelb et al., 1974). This should  
 128 be one possible explanation why nudging usually works quite well and the converged state is not  
 129 strongly affected by the choice of  $\mathbf{K}$ . However, when constructing  $\mathbf{K}$  (which units is  $s^{-1}$ ), the aim  
 130 is to obtain an estimator response faster than the time scale of the studied processes.

131 The BFN is an iterative algorithm which sequentially solves the forward model equations with a  
 132 feedback term to the observations (Eq. 1) and the backward model equations with an opposite sign  
 133 for the feedback term. The initial condition of the backward integration is the final state obtained  
 134 after integration of the forward nudging equation. At the end of each iteration a new estimation of  
 135 the system's initial state is obtained. The iterations are carried out until convergence is reached.

136 The BFN novelty with respect to conventional nudging methods is the model integration back-  
 137 ward in time. This allows to recover initial conditions as well as to use more than once the same  
 138 observations set. Consequently, the BFN may be seen as a sub-optimal iterative smoother.

139 Under the hypothesis of a linear model a variational interpretation is possible. In this case, if we  
 140 choose  $\mathbf{K} = k\mathbf{H}^T\mathbf{R}^{-1}$ , where  $\mathbf{R}$  is the observation error covariance matrix, and  $k$  is a scalar, the  
 141 solution of the estimation problem is a compromise between the minimization of the system's energy  
 142 and the minimization of the distance between the data and the model (Auroux, 2009).

143 However, the backward integration is problematic when the model is diffusive or simply not re-  
 144 versible. In the case of ocean models, there are two main aspects requiring the inclusion of diffusion:  
 145 i) the control of numerical noise, and ii) the modeling of sub grid-scale processes, i.e. to parameter-  
 146 ize the energy transfer from explicitly resolved to non-resolved scales. Indeed, diffusion naturally  
 147 represents a source of uncertainty in ocean forecasts, even for the purely forward model, and has  
 148 been investigated from the point of view of the optimal control theory in Leredde et al. (1999).

149 To address the problem of the backward model instability in this article the Diffusive Back and  
 150 Forth Nudging-DBFN (Auroux et al., 2011) is used. In this algorithm the sign of the diffusion term  
 151 remains physically consistent and only the reversible part of the model equations are really solved  
 152 backward. Practical consequences of this assumption are analysed in Sect 4. A similar solution was  
 153 proposed by Pu et al. (1997) and Kalnay et al. (2000) to stabilize their Quasi-Inverse Linear model.

154 To describe the DBFN algorithm, let us assume that the time continuous model satisfies dynamical  
 155 equations of the form:

$$156 \quad \frac{\partial \mathbf{x}}{\partial t} = \mathcal{F}(\mathbf{x}) + \nu \Delta \mathbf{x}, \quad \text{for} \quad 0 < t < T, \quad (2)$$

157 with an initial condition  $\mathbf{x}(0) = \mathbf{x}_0$ , where  $\mathcal{F}$  denotes the nonlinear model operator without diffusive  
 158 terms,  $\nu$  is a diffusion coefficient and  $\Delta$  represents a diffusion operator. If nudging is applied to the  
 159 forward system (2) it gives:

$$160 \quad \frac{\partial \mathbf{x}_k}{\partial t} = \mathcal{F}(\mathbf{x}_k) + \nu \Delta \mathbf{x}_k + \mathbf{K}(\mathbf{x}_{obs} - \mathcal{H}(\mathbf{x}_k)) \quad (3)$$

$$161 \quad \mathbf{x}_k(0) = \tilde{\mathbf{x}}_{k-1}(0), \quad 0 < t < T,$$

162 where  $k \in \mathbb{N}_{\geq 1}$  stands for iterations. Nudging applied to the backward system with the reversed  
 163 diffusion sign gives:

$$164 \quad \frac{\partial \tilde{\mathbf{x}}_k}{\partial t} = \mathcal{F}(\tilde{\mathbf{x}}_k) - \nu \Delta \tilde{\mathbf{x}}_k - \mathbf{K}'(\mathbf{x}_{obs} - \mathcal{H}(\tilde{\mathbf{x}}_k)) \quad (4)$$

$$165 \quad \tilde{\mathbf{x}}_k(T) = \mathbf{x}_k(T), \quad T > t > 0.$$

166 The system composed by equations (3) and (4) is the basis of the DBFN algorithm. They are iterated  
 167 until convergence.

168 Therefore, one important aspect of the DBFN algorithm is the convergence criterion. Ideally,  
 169 at convergence the nudging term should be null or small comparable to the other equation terms.  
 170 Otherwise, when the nudging is switched off, which is the case in the forecast phase, the system  
 171 may return to a state close to the background state or to a state which is not consistent to the one at  
 172 convergence. The convergence is calculated as:

$$173 \quad \frac{\|\mathbf{x}_k(t=0) - \mathbf{x}_{k-1}(t=0)\|}{\|\mathbf{x}_{k-1}(t=0)\|} \leq \epsilon, \quad (5)$$

174 where  $\|\bullet\|$  is the  $L_2$  norm, and the choice for  $\epsilon = 0.005$  is based on sensitivity tests (not presented  
 175 in this article).

176 If  $\mathbf{K}' = \mathbf{K}$  and the forward and backward limit trajectory are equal, i.e  $\tilde{\mathbf{x}}_\infty = \mathbf{x}_\infty$ , then taking the  
 177 sum between Eqs.(3) and (4) shows that  $\mathbf{x}_\infty$  satisfies the model equations without diffusion:

$$178 \quad \frac{\partial \mathbf{x}_\infty}{\partial t} = \mathcal{F}(\mathbf{x}_\infty) \quad (6)$$

179 while taking the difference between Eqs.(3) and (4) shows that  $\mathbf{x}_\infty$  satisfies the Poisson equation:

$$180 \quad \Delta \mathbf{x}_\infty = -\frac{\mathbf{K}}{\nu}(\mathbf{x}_{obs} - \mathcal{H}(\mathbf{x}_\infty)) \quad (7)$$

181 which represents a smoothing process on the observations for which the degree of smoothness is  
 182 given by the ratio  $\frac{\nu}{\mathbf{K}}$  (Auroux et al., 2011). We call attention to the fact that the convergence of the  
 183 BFN algorithm for transport equations exists only for the linear viscous transport equation and for  
 184 the non-linear inviscid transport equation under strong observability conditions (Auroux and Nodet,  
 185 2012). Therefore, we have no guarantee that the iterations are convergent and that the forward and  
 186 backward trajectory are the same at convergence for a Primitive Equation model. Nevertheless,  
 187 Eqs.(6) and (7) give an idea about how the DBFN works and about a possible relationship between  
 188 the solution at convergence and the observations.

189 The description of the used  $\mathbf{K}$  matrix is given in the Sect (5.1).

## 190 2.2 Four Dimensional Variational Method - 4DVar

191 Variational methods minimize a cost function that measures the distance between the estimated  
 192 state and the available observations. Let us assume that observations are available at every instant  
 193  $(t_i)_{1 \leq i \leq N}$ . Given a first guess  $\mathbf{x}^b$  of the initial state, the 4DVar algorithm will find an optimal initial

194 condition that minimizes the distance between the model trajectory and the observations in a given  
 195 assimilation window. This optimal state is found by minimizing the following cost function:

$$\begin{aligned}
 196 \quad J(\mathbf{x}_0) &= \frac{1}{2}(\mathbf{x}_0 - \mathbf{x}^b)^T \mathbf{B}^{-1}(\mathbf{x}_0 - \mathbf{x}^b) \\
 197 \quad &+ \frac{1}{2} \sum_{i=0}^N (\mathcal{H}_i[\mathcal{M}_{0,i}(\mathbf{x}_0)] - \mathbf{y}_i)^T \mathbf{R}_i^{-1} (\mathcal{H}_i[\mathcal{M}_{0,i}(\mathbf{x}_0)] - \mathbf{y}_i)
 \end{aligned} \tag{8}$$

198 where  $\mathbf{B}$  is the background error covariance matrix and  $\mathcal{M}_{0,i}$  represents the model integration from  
 199 time  $t_0$  to time  $t_i$ .  $\mathbf{R}_i, \mathcal{H}_i$  and  $\mathbf{y}_i$  are the observations error covariance matrix, the observation  
 200 operator and the available observations at time  $t_i$ , respectively.

201 The optimal initial state is found by solving:

$$202 \quad \nabla J(\mathbf{x}^a(t_0)) = 0 \tag{9}$$

203 The calculation of this gradient is done using the adjoint method proposed by Lions (1971) and  
 204 brought to the meteorological context by Le Dimet and Talagrand (1986).

205 If  $\mathcal{H}$  or  $\mathcal{M}$  are nonlinear, the solution of the problem is not unique, i.e. the functional (8) may  
 206 have multiple local minima, and the minimization procedure may not stop at the global minimum. To  
 207 overcome this problem, Courtier et al. (1994) proposed to solve a sequence of quadratic problems,  
 208 expecting this sequence would converge to the solution of the problem given by (8) and (9). This  
 209 algorithm is called the incremental 4Dvar. In this case, the cost function will not be minimized  
 210 with respect to the initial state but with respect to an increment  $\delta \mathbf{x}_0$  defined by  $\mathbf{x}_0 = \mathbf{x}^b + \delta \mathbf{x}_0$ . The  
 211 operators  $\mathcal{H}$  or  $\mathcal{M}$  are linearized in a neighborhood of  $\mathbf{x}^b$  as:

$$212 \quad \mathcal{M}_{0,i}(\mathbf{x}^b + \delta \mathbf{x}_0) \approx \mathcal{M}_{0,i}(\mathbf{x}^b) + \mathbf{M}_{0,i} \delta \mathbf{x}_0 \quad \forall i \tag{10}$$

$$213 \quad \mathcal{H}_i(\mathbf{x}^b + \delta \mathbf{x}_0) \approx \mathcal{H}_i(\mathbf{x}^b) + \mathbf{H}_i \delta \mathbf{x}_0 \quad \forall i \tag{11}$$

214 and the new cost function is given by:

$$215 \quad J(\delta \mathbf{x}_0) = \frac{1}{2} \delta \mathbf{x}_0^T \mathbf{B}^{-1} \delta \mathbf{x}_0 + \frac{1}{2} \sum_{i=0}^N (\mathbf{H}_i \mathbf{M}_{0,i} \delta \mathbf{x}_0 - \mathbf{d}_i)^T \mathbf{R}_i^{-1} (\mathbf{H}_i \mathbf{M}_{0,i} \delta \mathbf{x}_0 - \mathbf{d}_i) \tag{12}$$

216 where  $\mathbf{d}_i = \mathbf{y}_i - \mathcal{H}_i(\mathcal{M}_{0,i}(\mathbf{x}^b))$  is called the innovation vector. It is possible that after some iterations  
 217 of the minimizer the increments become too large and a new linearization of  $\mathcal{H}$  and  $\mathcal{M}$  should be  
 218 done. This gives rise to what is called the inner loop and outer loop iterations. The algorithm  
 219 implemented in NEMO, called NEMOVAR (Mogensen et al., 2009), uses this technics. It can be  
 220 summarized as follows:

–**Initialisation** :  $\mathbf{x}_0^0 = \mathbf{x}^b$   
–**While**  $k \leq k_{max}$  or  $\|\delta\mathbf{x}_0^{a,k}\| > \epsilon$  (**Outer Loop**)

**Do**

•  $\mathbf{d}_i^k = \mathbf{y}_i - \mathcal{H}_i(\mathcal{M}_{0,i}(\mathbf{x}_0^k))$

• Search the  $\delta\mathbf{x}_0^{a,k}$  that minimises (**Inner Loop**):

221

$$J(\delta\mathbf{x}_0^k) = \frac{1}{2}(\delta\mathbf{x}_0^k)^T \mathbf{B}^{-1}(\delta\mathbf{x}_0^k) \quad (13)$$

$$+ \frac{1}{2} \sum_{i=0}^N (\mathbf{H}_i \mathbf{M}_{0,i} \delta\mathbf{x}_0^k - \mathbf{d}_i^k)^T \mathbf{R}_i^{-1} (\mathbf{H}_i \mathbf{M}_{0,i} \delta\mathbf{x}_0^k - \mathbf{d}_i^k)$$

•  $\mathbf{x}_0^{k+1} = \mathbf{x}_0^k - \delta\mathbf{x}_0^{a,k}$

222

The description of the matrices  $\mathbf{B}$  and  $\mathbf{R}$  is given in the Sect (5.2).

### 223 3 Ocean Model and Experimental set-up

224 The ocean model used in this study is the ocean component of NEMO (Nucleus for European Mod-  
225 elling of the Ocean; Madec, 1996). This model is able to represent a wide range of ocean motions,  
226 from the basin scale up to the regional scale. Currently, it has been used in operational mode by the  
227 French Mercator Océan group (<http://www.mercator-ocean.fr>) and the European Center for Medium  
228 Range Weather Forecast (ECMWF).

229 The model solves six prognostic equations, namely the momentum balance, the hydrostatic equi-  
230 librium, the incompressibility equation, the heat and salt conservation equations and a nonlinear  
231 equation of state which couples the two tracers to the fluid fields. In this study, a linear free surface  
232 formulation is used along with the approach developed by Rouillet and Madec (2000) to filter out the  
233 external gravity waves.

234 Equations are discretized using spherical coordinates in a Arakawa C grid. The model advances in  
235 time using a leap-frog scheme for all terms except for the vertical diffusive terms, which are treated  
236 implicitly. At every time step the model uses a Robert-Asselin (RA) temporal filter to damp the  
237 computational mode. The leap-frog scheme followed by the RA filter leads to a first order temporal  
238 scheme (Williams, 2009). Spatial discretization uses a centered second order formulation for both  
239 the advective and the diffusive terms.

240 The double gyre configuration, extensively used to study jet instabilities (Chassignet and Gent,  
241 1991; Primeau, 1998; Chang et al., 2001), meso and submeso-scale dynamics (Levy et al., 2010)  
242 and data assimilation methods (Molcard et al., 2004; Krysta et al., 2011; Cosme et al., 2010), is used  
243 for the present study. The double gyre configuration simulates the ocean middle latitude dynamics  
244 and has the advantage of being simple, when compared to real applications, but still considering full  
245 dynamics and thermodynamics.

246 In our experiments we use a homogeneous horizontal grid with a 25km resolution and a verti-

247 cal resolution ranging from 100m near the upper surface to 500m near the bottom. The bottom  
 248 topography is flat and the lateral boundaries are closed and frictionless. The only forcing term  
 249 considered is a constant wind stress of the form  $\tau = \left( \tau_0 \cos\left(\frac{2\pi(y-y_0)}{L}\right), 0 \right)$ , where  $y$  is the lati-  
 250 tude geographic coordinate with  $y_0 = 24^\circ$  and  $y_0 \leq y \leq 44^\circ$ ,  $L = 20^\circ$  and  $\tau_0 = -0.1N/m^2$ . Hori-  
 251 zontal diffusion/viscosity are modeled by a bilaplacian operator meanwhile a laplacian operator is  
 252 used in the vertical. They all use constant coefficients in time and space:  $\nu_h^{u,v} = -8 \times 10^{10} m^4/s$   
 253 and  $\nu_v^{u,v} = 1.2 \times 10^{-4} m^2/s$  for the momentum equations and  $\nu_h^{t,s} = -4 \times 10^{11} m^4/s$  and  $\nu_v^{t,s} =$   
 254  $1.2 \times 10^{-5} m^2/s$  for temperature and salinity. The initial condition is similar to that used by Chas-  
 255 signet and Gent (1991) and consists of a homogeneous salinity field of 35psu and a temperature field  
 256 created to provide a stratification which has a first baroclinic deformation radius of 44.7km. Velocity  
 257 and sea surface height (SSH) fields are initially set to zero.

258 This double gyre configuration is currently used as the NEMO data assimilation demonstrator and  
 259 as the experimentation and training platform for data assimilation activities (Bouttier et al., 2012).  
 260 For the present work, the model was integrated for 70 years, in order to reach the statistical steady  
 261 state. Afterwards, ten years of free model run were performed, that were used to calculate the re-  
 262 gression models which are used to calculate the nudging matrix  $\mathbf{K}$  (see Sect 5.1), and then two  
 263 additional years were finally completed to be used as the truth, from which the observations were  
 264 extracted.

#### 265 4 The backward integration without Nudging: Practical aspects

266 The backward model uses exactly the same numerical scheme as the forward model. Since most  
 267 of the model is solved using centered finite differences, the inverse version of the discretized model  
 268 is similar to the discrete version of the inverse continuous model. The only distinction between  
 269 the forward and the backward model is the change in the sign of the diffusive terms when stepping  
 270 backwards, this making the backward integration stable. If this is not taken into account the model  
 271 blows up after a few days.

272 Reversing the diffusion sign in the backward model is a numerical artifact and being so its effects  
 273 should be carefully analysed. In this section, the backward integration accuracy is studied, as well  
 274 as its sensitivity with respect to the choice of the diffusion coefficient. The errors are analysed  
 275 calculating the L2 error norm at the end of one forward-backward integration relative to a typical  
 276 one day model variation:

$$277 R_{\text{err}} = \frac{\|\mathbf{x}(0) - \tilde{\mathbf{x}}(0)\|}{\langle \|\mathbf{x}(t + \Delta t) - \mathbf{x}(t)\| \rangle} \quad (14)$$

278 where  $\Delta t = 1\text{day}$  and the brackets represent the empirical mean.

279 Figure 1 shows the global error,  $R_{\text{err}}$ , for different window sizes. The errors grow linearly with  
 280 the window size for all variables. Temperature is the most affected variable, followed by sea level  
 281 and velocities. Temperature errors exceed 18 times a typical one-day variation for the 30 days exper-

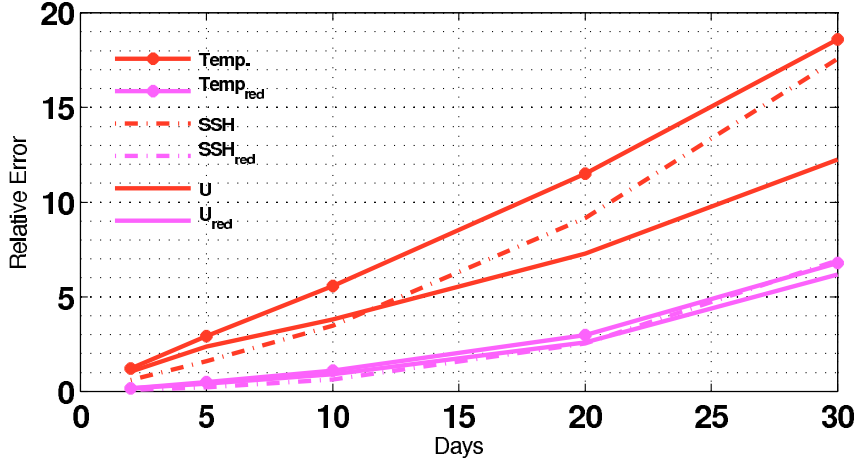


**Fig. 1.** Errors on the initial condition after one forward-backward model integration perfectly initialized and without nudging. Red curves were obtained using the same diffusion coefficients as in the reference experiment ( $\nu_h^{u,v} = -8 \times 10^{10} m^4/s$  and  $\nu_h^{t,s} = -4 \times 10^{11} m^4/s$ ) and magenta curves were obtained using reduced diffusion ( $\nu_h^{u,v} = -8 \times 10^9 m^4/s$  and  $\nu_h^{t,s} = -8 \times 10^{10} m^4/s$ ). The abscissa represents the length of the time window.

282 iment and 1.2 times for the 2 days. The use of reduced diffusion/viscosity reduces the  
 283 errors to 6.8 and 0.16 times the one-day variation for 30 and 2 days experiments, respectively. Ve-  
 284 locities errors were reduced by 50% for 30 days and 85% for 2 days, while ssh errors were reduced  
 285 by 60% and 88% for 30 and 2 days, respectively.

286 As shown on Fig. 2 velocity and temperature errors are depth-dependent. Whereas for velocity  
 287 they are larger at the surface and decrease with depth, for temperature they are larger in the ther-  
 288 mocline. In the cases for which the forward-backward integrations use the same diffusion/viscosity  
 289 coefficients as in the reference simulation, the temperature errors at thermocline depths exceed 3  
 290 times the typical one day variation for the 5 days experiments and reaches 15 times for 20 days ex-  
 291 periments. Considering the velocities, errors are proportional to 4 one-day variations for the 5 days  
 292 experiment and to 8 one-day variations for the 20 days experiments. For time windows of 10, 20 and  
 293 30 days, velocities at the thermocline depths start to be influenced by temperature errors.

294 Reduction of the diffusion/viscosity coefficients greatly reduced the errors especially in the ther-  
 295 mocline for the temperature and at the surface for the velocity. It can be noted that when the diffusion  
 296 coefficient is decreased the errors converge to a limit. This limit changes with respect to the window  
 297 length and should be related to the diffusion required to stabilize the numerical method, which is of  
 298 second order in our case, and hence oscillatory. Therefore, there is a compromise between the errors  
 299 induced by the extra diffusion and errors due to spurious oscillations.

300 Numerical errors were assessed by changing the model time step from 900s to 90s. The resulting  
 301 errors (not shown) do not change, suggesting that the errors induced by the diffusion are domi-



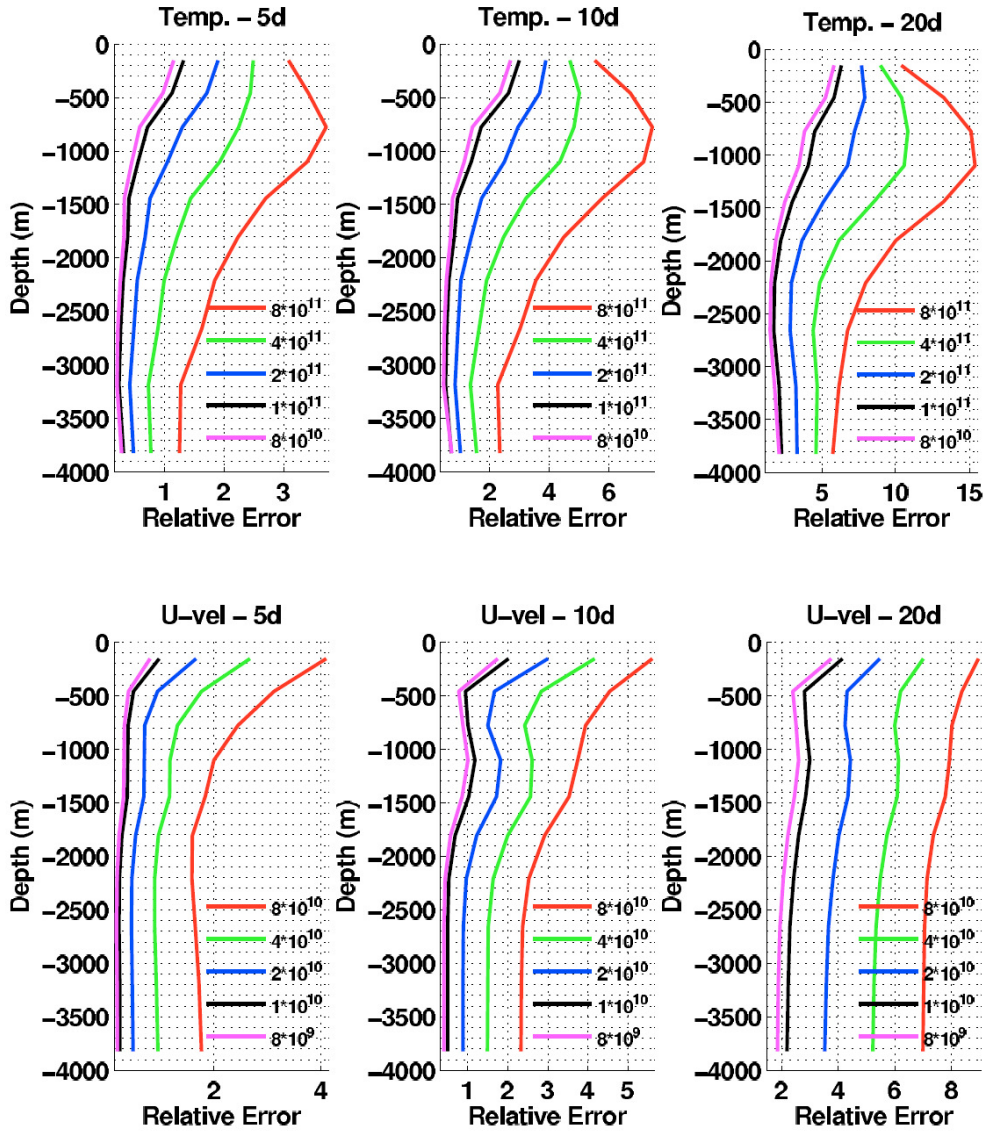


**Fig. 2.** Vertical profiles of relative errors on the initial condition after one forward-backward model integration without nudging. Each color refers to an experiment performed using the diffusion coefficient indicated in the figures legend. Red curves were obtained using the same diffusion coefficients as in the reference experiment. Top panel: temperature errors; bottom panel: zonal velocity errors. The length of the time window is indicated in the title of each figure.

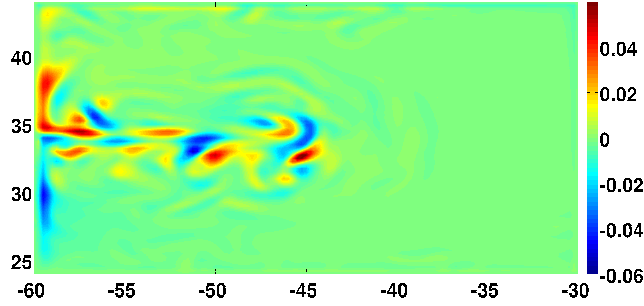


Fig. 3. Sea level errors after one forward-backward model integration. The time window is of 10 days.

302 nant. On the one hand, this is important because the complete rewriting of the model’s code can be  
 303 difficult, similarly to the adjoint model programming used by the 4Dvar, but on the other hand if  
 304 the assimilation cannot control the diffusion errors it may represent a fundamental problem of the  
 305 method when it is applied to non-reversible geophysical systems such as the ocean.

306 Figure 3 shows the spatial structures of the sea level error for the 10 days experiment. The errors  
 307 are highly variable in space, being larger along the main jet axis. This is probably due to the fact that  
 308 the backward integration smooths the gradients and so the largest errors are found near the fronts.  
 309 Therefore, the errors structures may be of high variability in space and time since they are state  
 310 dependent.

311 Figure 4 shows the surface kinetic energy spectrum calculated from the experiment employing  
 312 the reference diffusion coefficient and a reduced diffusion coefficient. The backward integration  
 313 introduces an extra diffusion, coarsening the effective model resolution, which is defined as the por-  
 314 tion of the spectra for which there is a change in the spectrum slope. In the reference simulation the  
 315 effective model resolution is estimated to be 190km, which is coherent with the  $\approx 7 \times \Delta x$  estimation  
 316 of Skamarock (2004).

317 The longer the time window the greater the portion of the spectra affected. For the experiment  
 318 employing the reference diffusion coefficient, the divergence between the true spectra and the spec-  
 319 tra obtained from the backward integration is observed at 126, 314 and 627km for 5, 10 and 20 days  
 320 experiments, while for the experiments considering a reduced diffusion coefficient there is almost  
 321 no differences for the 5 days experiment, and the divergence is observed at 126 and 314km for the  
 322 10 and 20 days experiments. If on the one hand using the reduced diffusion helps to keep the en-  
 323 ergy distribution coherent with the true distribution, on the other hand it creates noise in the range  
 324 of 126km to 25km. This confirms that there is a trade-off between the errors due to the excessive  
 325 smoothing and the errors due to high frequency numerical modes.

326 In this section we have seen that there are large backward-errors induced by over-diffusion.  
 327 Therefore, short time windows with reduced diffusion coefficients would be preferable to be used  
 328 in DA experiments. Two regions have to be cautiously analyzed: the surface and the thermocline.

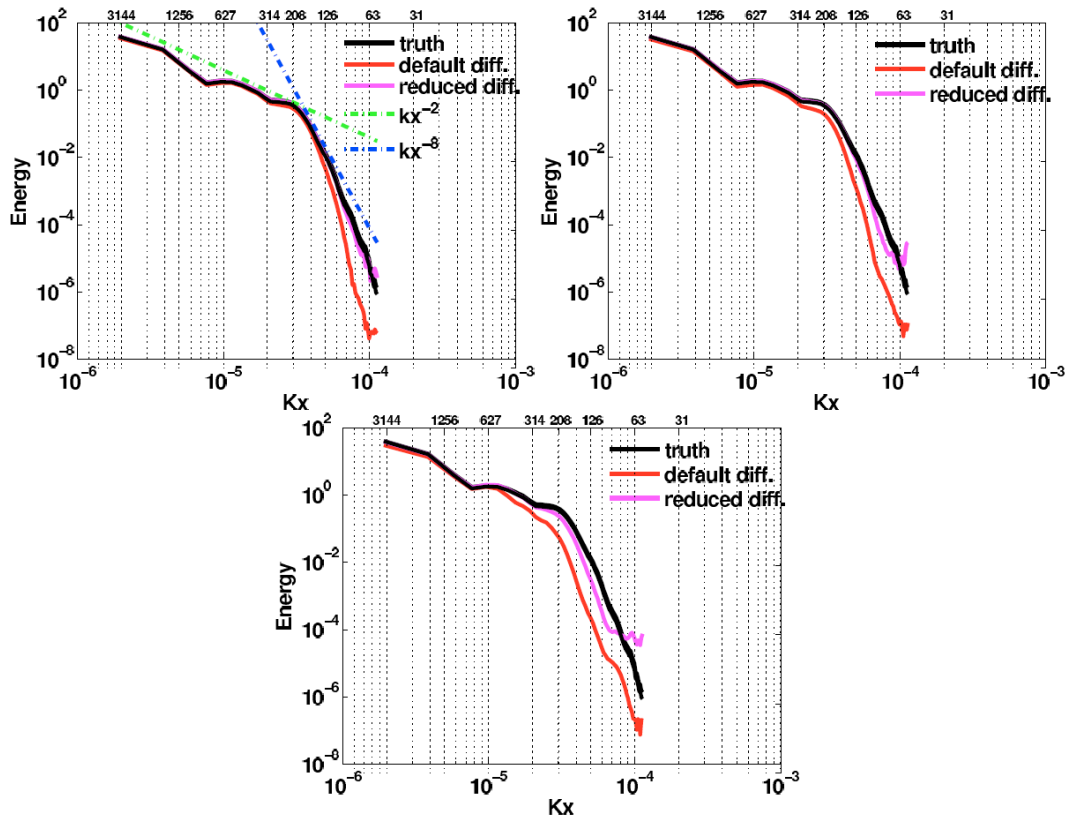


**Fig. 4.** Kinetic energy mean power spectra calculated using the first layer velocity fields. Black curves represent the “true” initial condition power spectra; Red curves represent the power spectra calculated after one forward-backward iteration without the nudging term and employing the reference diffusion coefficient; Magenta curves represent the power spectra calculated after one forward-backward iteration without the nudging term and employing a reduced diffusion coefficient. Top left: 5 days assimilation window. Top right: 10 days assimilation window. Bottom: 20 days assimilation window. In the bottom abscissa the ticklabels stand for longitudinal wave-number ( $rad/m$ ) while in the top abscissa the ticklabels stand for the corresponding wavelengths in  $km$  units.

329 Surface layers are prone to feature errors due to their role on the wind energy dissipation while at  
 330 the thermocline strong density gradients contribute to high diffusion rates.

## 331 **5 Data Assimilation experiments**

### 332 **5.1 Prescription of the DBFN gain**

333 In this study the matrix  $\mathbf{K}$  is composed by the two operations: first the observed variables are  
 334 updated using a prescribed weight and subsequently the other state variables are calculated using  
 335 linear regression. More precisely, defining  $\mathbf{y} = \mathcal{H}(\mathbf{x})$  as the observed part of the state vector, the  
 336 first step may be written as:

$$337 \mathbf{y}^a = \mathbf{y}^b + \Theta(\mathbf{x}^{obs} - \mathbf{y}^b) \quad (15)$$

338 where the superscripts  $a$  and  $b$  denote the analysed field and the background field, respectively. The  
 339 prescribed weight is given by:

$$340 \Theta = \frac{\sigma_m^2}{\sigma_m^2 + \gamma\sigma_o^2} \quad (16)$$

341 where  $\sigma_m^2$  is the mean spatial value of SSH variance calculated from the free model run,  $\sigma_o^2$  is the  
 342 observation error variance and  $\gamma$  is an inflation factor which should be considered since each set of  
 343 observations is used more than once in the DBFN iterations. The used values for these parameters  
 344 are  $\sigma_m = 0.017m$  and  $\sigma_o = 0.03m$  consistently with the perturbations added to the observations (see  
 345 Sect. 5.4) and  $\gamma = 18$ .

346 Then, the non-observed variables are updated by using a regression equation of the form:

$$347 \mathbf{x}^a = \mathbf{x}^b + \hat{\mathbf{B}}^{PLS}(\mathbf{y}^a - \mathbf{y}^b) \quad (17)$$

348 where  $\hat{\mathbf{B}}^{PLS}$  is the Partial Least Squares (PLS) regression coefficients which are described below.  
 349 It is worth noting that in Sect.(6) we also apply this update scheme to an ordinary direct nudging  
 350 experiment. In this case  $\gamma$  is equal to one.

351 The PLS can be seen as an improvement to the Ordinary Least Square (OLS) regression. The most  
 352 important difference between OLS and PLS is that the later assumes that the maximum information  
 353 about the non-observed variables is in those directions of the observed space which simultaneously  
 354 have the highest variance and the highest correlation with the non-observed variables.

355 In the PLS description (Tenenhaus, 1998),  $\mathbf{Y} \in \mathbb{R}^{n \times M}$  is considered as the observed or predictor  
 356 variables and  $\mathbf{X} \in \mathbb{R}^{n \times N}$  as the non-observed or response variables. In our notation  $n$  is the sample  
 357 size and  $M$  and  $N$  are respectively the size of the state space of  $\mathbf{Y}$  and  $\mathbf{X}$ . Besides,  $\mathbf{Y}$  and  $\mathbf{X}$  are  
 358 centered and have the same units. The PLS regression features two steps: a dimension reduction step  
 359 in which the predictors from matrix  $\mathbf{Y}$  are summarized in a small number of linear combinations  
 360 called "PLS components". Then, that components are used as predictors in the ordinary least-square

361 regression.

362 The PLS as well as the principal component regression can be seen as methods to construct a  
363 matrix of  $p$  mutually orthogonal components  $\mathbf{t}$  as linear combinations of  $\mathbf{Y}$  :

$$364 \quad \mathbf{T} = \mathbf{Y}\mathbf{W}, \quad (18)$$

365 where  $\mathbf{T} \in \mathbb{R}^{n \times p}$  is the matrix of new components  $\mathbf{t}_i = (t_{1i}, \dots, t_{ni})^T$ , for  $i = 1, \dots, p$ , and  $\mathbf{W} \in \mathbb{R}^{M \times p}$   
366 is a weight matrix satisfying a particular optimality criterion.

367 The columns  $\mathbf{w}_1, \dots, \mathbf{w}_p$  of  $\mathbf{W}$  are calculated according to the following optimization problem:

$$368 \quad \mathbf{w}_i = \operatorname{argmax}_{\mathbf{w}} \{ \operatorname{cov}(\mathbf{Y}\mathbf{w}, \mathbf{X})^2 \} \quad (19)$$

369 subject to  $\mathbf{w}_i^T \mathbf{w}_i = 1$  and  $\mathbf{w}_i^T \mathbf{Y}^T \mathbf{Y} \mathbf{w}_j = 0$  for  $j = 1, \dots, i-1$ .

370 The PLS estimator  $\hat{\mathbf{B}}^{PLS}$  is given by:

$$371 \quad \hat{\mathbf{B}}^{PLS} = \mathbf{W}(\mathbf{W}^T \mathbf{Y}^T \mathbf{Y} \mathbf{W})^{-1} \mathbf{W}^T \mathbf{Y}^T \mathbf{X} \quad (20)$$

372 An immediate consequence of Eq. (20) is that when  $\mathbf{W} = \mathbf{I}$  the Ordinary Least Squares solution is  
373 obtained.

374 The number of components  $p$  is chosen from cross-validation. This method involves testing a  
375 model with objects that were not used to build the model. The data set is divided in two contiguous  
376 blocks; one of them is used for training and the other to validate the model. Then the number of  
377 components giving the best results in terms of mean residual error and estimator variance is sought.

378 The weight  $\Theta$  and the regression model  $\hat{\mathbf{B}}^{PLS}$  are kept constant over the assimilation cycles  
379 and the correction steps (15) and (16) are applied at the end of the loop of time. Thus, our updat-  
380 ing scheme can be seen as a rough approximation of the two steps update for EnKF presented by  
381 Anderson (2003).

## 382 5.2 The 4Dvar background term configuration

The 4Dvar considers a background term of the form:

$$J_b = \frac{1}{2} (\delta \mathbf{x}_0^k)^T \mathbf{B}^{-1} (\delta \mathbf{x}_0^k)$$

383 where  $\mathbf{B}$  is the background error covariance matrix. This term is also known as a regularization term  
384 in the sense of Tikhonov. It is specially important when there is not enough observation to determine  
385 the problem.

386 The  $\mathbf{B}$  matrix is supposed to model the spatial covariance of the background errors of a given vari-  
387 able as well as the cross-covariance between the errors of different variables. Since the state space is  
388 too big, it is impossible to store the entire covariance matrix. Therefore, Derber and Bouttier (1999)  
389 have proposed the decomposition of the multivariate problem into a sequence of several univariate  
390 problems. This is accomplished by decomposing the variables into a balanced component and an



420 is closer to the true state than the very first background field. This usually reduces the number of  
421 iterations needed by the algorithms to reach convergence.

422 The length of the Data Assimilation window (DAw) used in the reference experiments (Sect. 6.1)  
423 is 10 days. For the sensitivity experiments presented in the Sect 6.2 the lengths of the the assimilation  
424 window are 5 days and 30 days.

## 425 **5.4 Observation network**

426 In this article, every four days an observation network simulating Jason-1 satellite density sample is  
427 available. The data is perturbed with white Gaussian noise with standard deviation equals to  $3cm$ .  
428 With this observation network a new set of 5000 observations is available every four days.

429 The data assimilation problem we proposed to solve is to recover the full model state at the begin-  
430 ning of the assimilation window. The model state space is composed of five variables: sea surface  
431 height ( $\eta$ ), meridional and zonal velocities ( $u$  and  $v$ ), temperature and salinity ( $temp$  and  $salt$ ).  
432 Since we have a horizontal mesh of size  $81 \times 121$  and 11 vertical layers the total size of the state  
433 space is 116640. Therefore, the problem is undetermined, since the observations represent only a  
434 4% of the total state space. This means that the background term, and accordingly the  $B$  matrix  
435 for the 4Dvar and the regression model  $\hat{B}^{PLS}$  for the DBFN, have quite a strong importance on the  
436 method performances since they project the increments of the observed variables onto the numerous  
437 non-observed variables.

## 438 **6 Data Assimilation Results**

### 439 **6.1 Reference experiment**

440 In this section the results produced by the DBFN, the 4Dvar method, the Ordinary Nudging (ONDG)  
441 and the control experiment are presented. All assimilation methods include the five prognostic vari-  
442 ables in the state vector. This is possible thanks to the PLS regression method in the case of the  
443 DBFN and ONDG and thanks to the multivariate balance operator  $G$  in the case of the 4Dvar ex-  
444 periments. The diffusion and viscosity coefficients used in the DBFN experiments are those which  
445 produced the smaller errors in the experiments without Nudging, as reported in Sect 4.

446 First the minimization performance of the 4Dvar implementation is analysed. Figure 5 shows the  
447 reduction of the cost function gradient for the 4Dvar and the reduction of the relative error of the  
448 zonal velocity for the DBFN, both of them for the first assimilation cycle. 4Dvar takes 26 iterations  
449 to approximately achieve the optimality condition  $\nabla J = 0$ . This represents 3 times the number of it-  
450 erations required by the DBFN to converge, i.e., after which the errors cease to decrease. Moreover,  
451 the 4Dvar numerical cost is more than 3 times the DBFN cost since one execution of the adjoint  
452 model costs four times the cost of the direct model in terms of CPU time.

453 We note that the minimum error for the DBFN is reached after 9 iterations. This is quite consis-

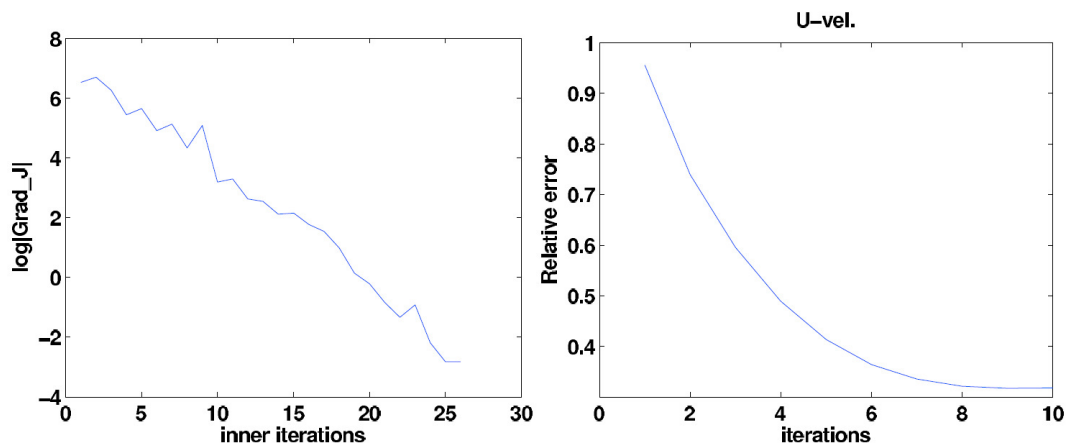


Fig. 5. Figure shows the gradient of the cost function after each inner iteration (left) and the reduction of the relative error for zonal velocity for the DBFN experiment (right).

454 tent with our choice  $\gamma = 18$ , since theoretically it allows the use of the same set of observations for  
 455 18 times.

456 Figure 6 shows the root mean squared (rms) error for the control experiment (without assimila-  
 457 tion), the experiment using the direct nudging with PLS regression (ONDG), the DBFN and the  
 458 4Dvar. The DBFN errors for the velocity and SSH converge to their asymptotic values after the  
 459 first assimilation cycle while for ONDG and 4Dvar errors stop decreasing after 100 and 200 days,  
 460 respectively. This is a benefit of the iterations performed by the DBFN when model and data are  
 461 quite different. Among the experiments conducted, the DBFN produced the smallest errors for all  
 462 variables, except for the zonal velocity, for which the 4Dvar has slightly smaller errors. The ONDG  
 463 also showed good performance, but with errors larger than the DBFN and 4Dvar errors.

464 With respect to the vertical error (Fig. 7), the DBFN and the ONDG performed better for the  
 465 upper ocean than 4Dvar. Clearly, the PLS also corrects the deep ocean velocity, but less accurately  
 466 than 4Dvar. The first error mode is the barotropic one, i.e. it has the same sign over all depths, and  
 467 accounts for 97% of the error variability for 4Dvar, 96% and 93% for DBFN and ONDG, respec-  
 468 tively. Although the first mode is the barotropic one for all methods, the 4Dvar barotropic mode of  
 469 error is out of phase with respect to the PLS barotropic mode. This reflects the better performance  
 470 of the 4Dvar for the deep ocean and the better performance of the DBFN and ONDG for the upper  
 471 ocean.

472 The second mode, which accounts for almost all the remaining variability, has a sign inversion  
 473 with depth and is found especially over the main axis of the jet. In this region the deep ocean veloc-  
 474 ities are overestimated due to spurious covariances between the SSH and the deep ocean velocities.

475 The way both methods correct the model depends on the  $B$  matrix in the 4Dvar algorithm and  
 476 on the regression model  $\hat{B}^{PLS}$  in the DBFN. It means that results may be different if another ap-



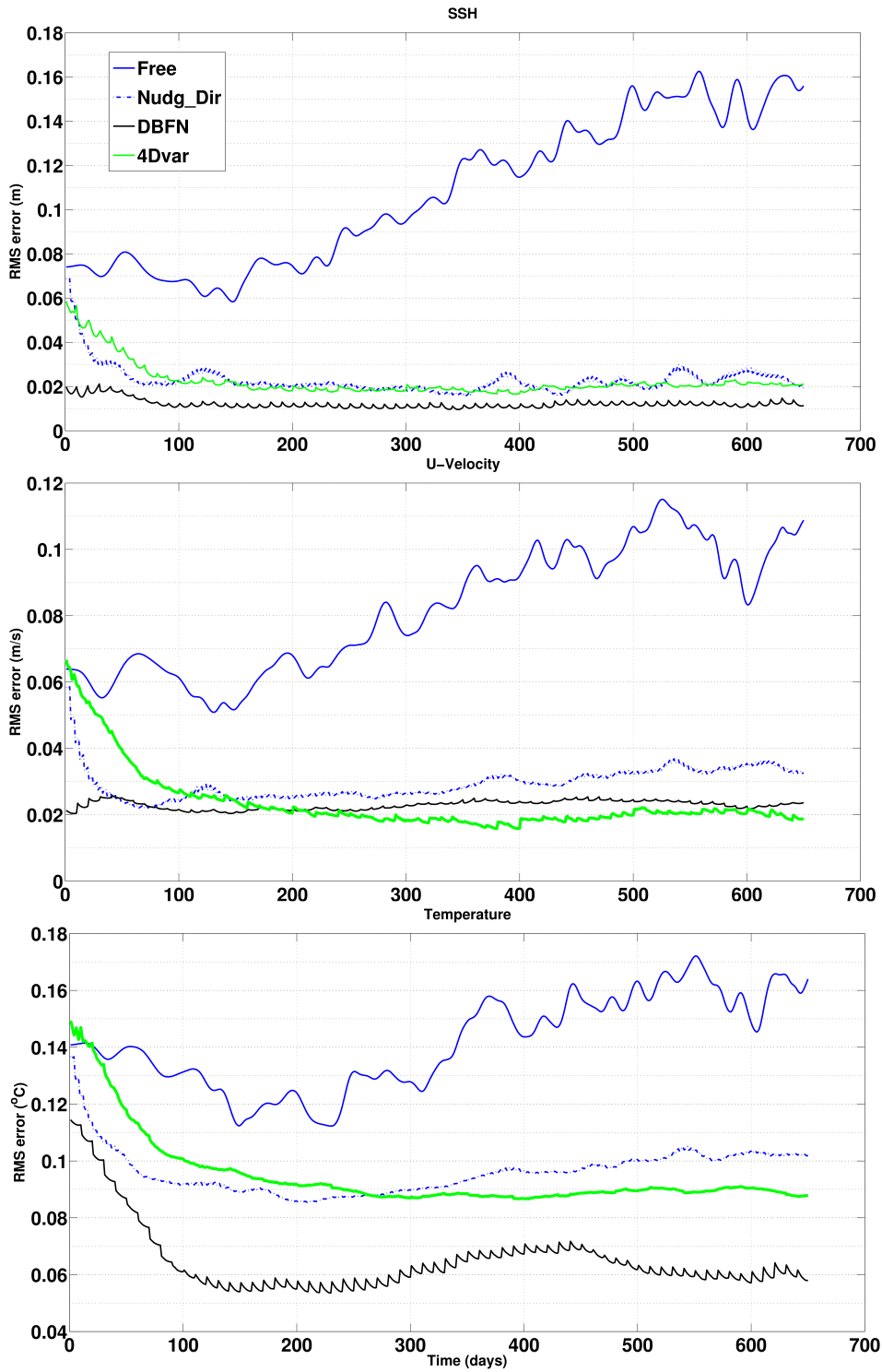


**Fig. 6.** The figure shows errors of the SSH (top panel), the zonal velocity (middle panel) and the temperature (bottom panel).

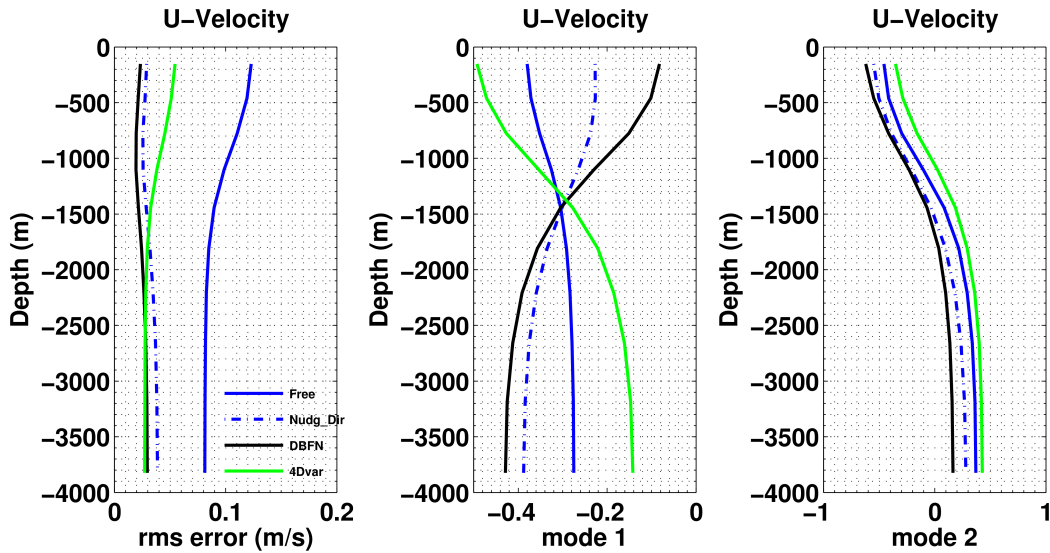


Fig. 7. Vertical profiles of rms error in zonal velocity (Left panel) and first (middle panel) and second (right panel) eof error modes calculated using forecast from day 200 to day 720.

477 proximation of  $B$  and another model regression model are used. Perhaps the main conclusion of  
 478 this comparison is that the DBFN, which is easier to implement and cheaper to execute, can produce  
 479 results similar to 4Dvar. Also, it is shown that iterations is an important aspect of the method. Iter-  
 480 ations compensate for the lack of a priori information on the model errors as well as filter out noise  
 481 in observations. The latter must be connected to the diffusive character of the algorithm. Moreover,  
 482 the iterations allows us to put information from the observations into the model, without causing  
 483 initialization problems since the nudging gain can be taken smaller than the one used for the direct  
 484 nudging due to the possibility of using more than once the same set of observations.

485

## 486 6.2 Sensitivity experiments

487 Sensitivity tests with respect to the length of the DA<sub>w</sub> are presented. As we have shown in Sect. 4,  
 488 the accuracy of the backward model is inversely proportional to the length of the DA<sub>w</sub>. Therefore,  
 489 in this section we present experiments using a DA<sub>w</sub> of five days and thirty days. The experiments  
 490 configuration is similar to those presented in the previous section.

491 Figure 8 shows the evolution of the rms errors for the zonal velocity and temperature during the  
 492 DBFN iterations over the first assimilation cycle, for three DA<sub>w</sub> (including the ten day-window used  
 493 previously). When considering only one iteration, the best results were obtained with the 30 days-  
 494 window experiment. This is a consequence of the asymptotic character of the Nudging method: the  
 495 longer the assimilation window, the more observations accounted for, the smaller the error. This

496 changes when several iterations are considered. The observed divergence for the 30 days-window is  
 497 due to the errors induced by the over-diffusion that induce great increments, which by their nature,  
 498 are not modelled by the ensemble of model states used to construct the regression model.

Figure 9 shows the rms error for the DBFN and 4Dvar experiments for three DAW: 5, 10 and

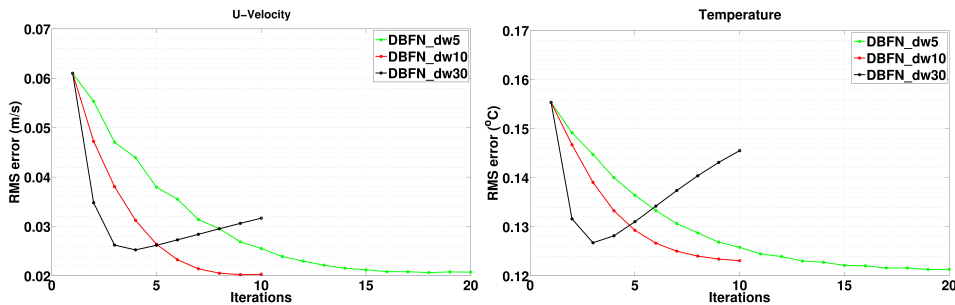


**Fig. 8.** Evolution of the rms errors for the zonal velocity and temperature during the DBFN iterations over the first assimilation cycle, for three DAW: 5, 10 and 30 days.

499  
 500 30 days. The methods exhibited comparable performance depending on the length of the DAW. For  
 501 the DBFN the 5 and 10 days DAW provided better results than the 30 days window, while for the  
 502 4Dvar the 30 days window provided the best estimation in terms of rms error. The DBFN and 4Dvar  
 503 experiments using the 30 and 5 days DAW, respectively, failed to identify the initial conditions since  
 504 their SSH rms errors are greater than the observation error standard deviation. The poor performance  
 505 of the 4Dvar for the 5 days DAW is related to spurious increments due to the fact that in one assim-  
 506 ilation window there is only one set of observation available. If this set is at the end of the window  
 507 this can complicate the minimization process and the iterations may stop before convergence.

508 Figure 10 shows the time evolution of vertical profiles of horizontally layer-wise averaged rms error  
 509 error of zonal velocities for the DBFN and 4Dvar experiments. The 4Dvar profits of the longer DAW  
 510 to spread the observation to the 3-dimensional variables. This is done by the iterations of the direct  
 511 model and by the  $B$  matrix. For the DBFN experiments, after one year of data assimilation the  
 512 errors in the deep ocean start to grow. This is due to the high variance of the PLS estimator for deep  
 513 layers. The problem becomes more evident on the second year because at this stage the observa-  
 514 tions are farther from the model states used to construct the regression coefficients. Therefore, this  
 515 mean that this behavior is not intrinsic to the DBFN algorithm and its diffusive aspects, but due to  
 516 our implementation. Ideally, the regression model should evolve in time, similarly to the Kalman  
 517 Filter scheme. The 4Dvar has good performance at the deep ocean thanks to the use of a vertical  
 518 localization with a length scale of  $1500m$ .

519 Next we investigate which scales are better represented by each assimilation method. This is done  
 520 by comparing the surface kinetic energy spectrum and the deep ocean kinetic spectrum produced by  
 521 each method. The Fig.(11) shows that the effective resolution of the model is not affected by the  
 522 diffusive character of the DBFN algorithm. It is clear that there is a reduction of the energy for the

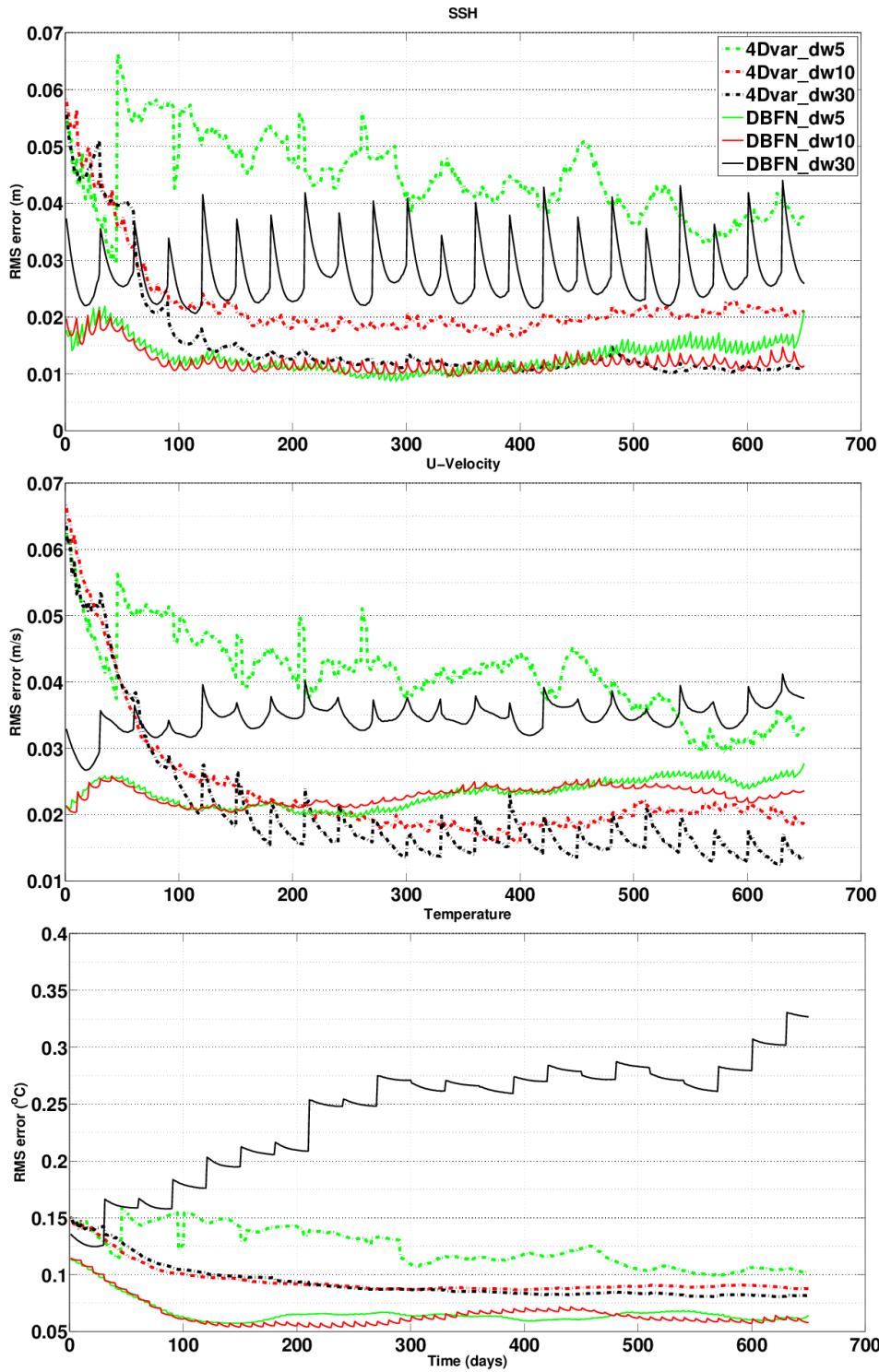
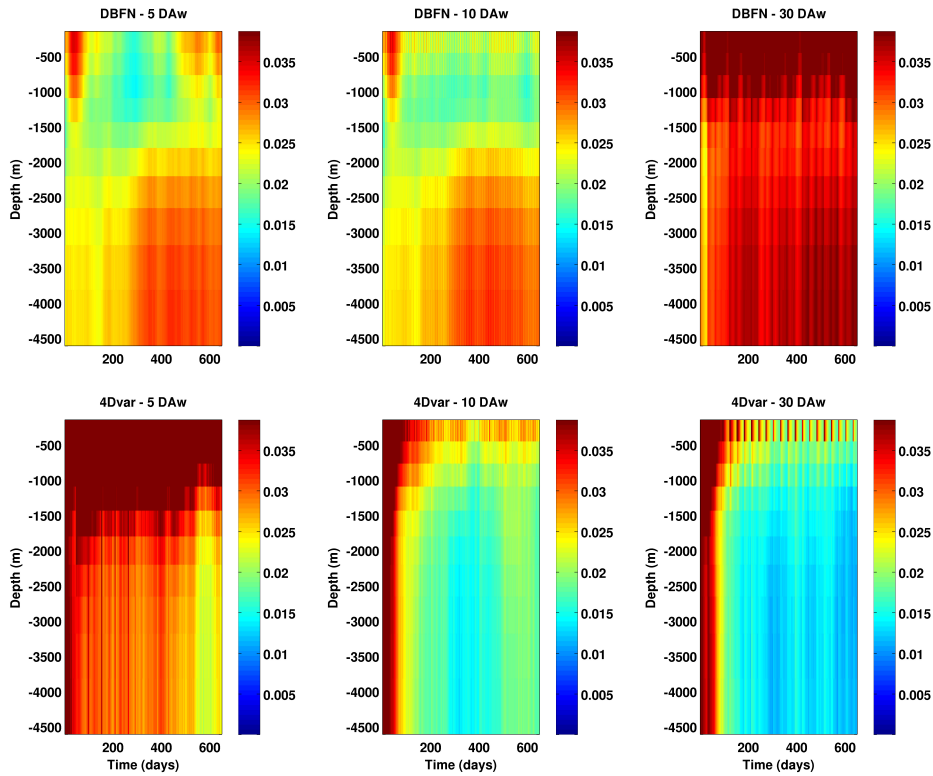


Fig. 9. RMS errors on SSH (top panel), zonal velocity (middle panel) and temperature (bottom panel) from DBFN and 4Dvar experiments with DAW of 5, 10 and 30 days.



**Fig. 10.** Time evolution of vertical profiles of horizontally layer-wise averaged rms error of zonal velocities for the DBFN (top panels) and 4Dvar (bottom panels) experiments. Units are in ( $m/s$ ).

523 scales close to the grid scale, but the energy contained in scales greater than  $7 \times \Delta x$  is not affected.  
 524 It means that the diffusion-induced errors presented in Sect 4 are "controlled" by the assimilation of  
 525 sea surface height observations.

526 There is no great difference between the DBFN and 4Dvar surface spectrum for the assimilation  
 527 windows shorter than 30 days, which once more proves the reliability of the DBFN for the assim-  
 528 ilation of oceanic observations. The energy spectra for the deep ocean velocities produced by the  
 529 DBFN contains more energy than the true spectrum independently of the used DAw. This confirms  
 530 that the deep ocean velocity errors are due to the high variance of the PLS regression model.

531

## 532 7 Conclusions and perspectives

533 This study used the NEMO general circulation model in a double gyre configuration to investigate  
 534 the Diffusive Back and Forth Nudging performance under different configurations of the data assim-  
 535 ilation window and to compare it with 4Dvar.

536 It has been shown that the reliability of the backward integration should be carefully examined  
 537 when the BFN/DBFN is applied to non-reversible systems. This should support the choice of the

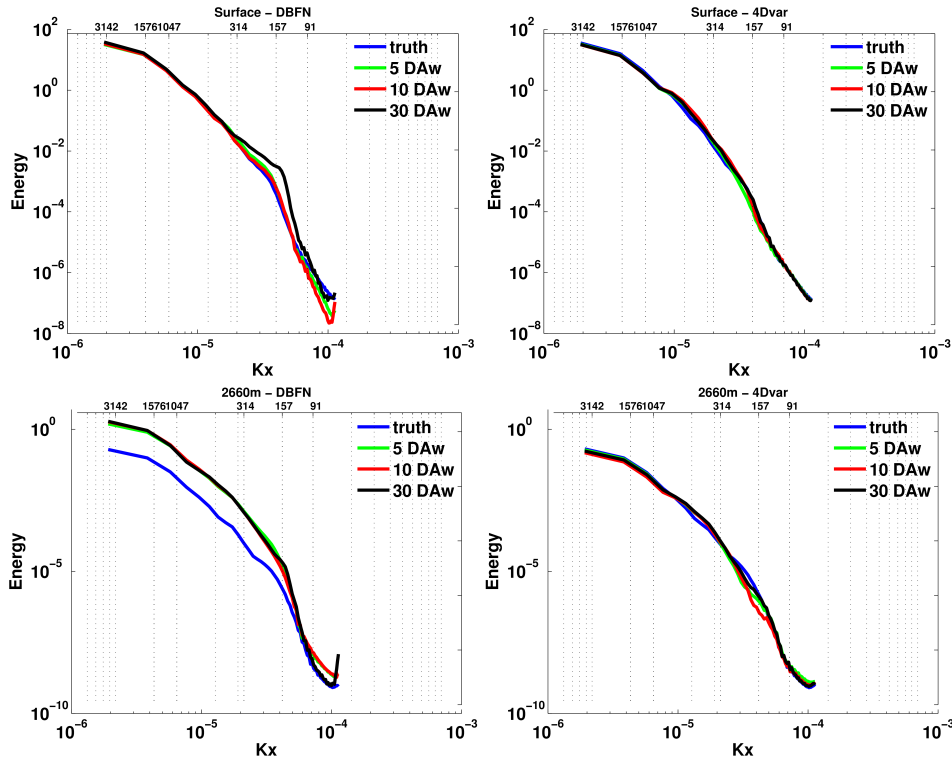


**Fig. 11.** Kinetic energy mean power spectra calculated using the first layer (top) and a layer at 2660m (bottom) and using the 650 days of the assimilation experiments using the DBFN (left) and the 4Dvar (right). Blue curves represent the “true” power spectra; Green curves represent the power spectra calculated for the 5 days DAw; Red curves represent the power spectra calculated for the 10 days DAw and Black curves represent the power spectra calculated for the 30 days DAw. In the bottom abscissa the tick-labels stand for longitudinal wave-number ( $rad/m$ ) while in the top abscissa the tick-labels stand for the corresponding wavelengths in  $km$  units.

538 assimilation window and identify whether the available observations are sufficient to control the er-  
 539 rors induced by the non-reversible terms of the model equations. In this article we have shown that  
 540 the DBFN might be used for the assimilation of realistically distributed ocean observations, despite  
 541 the limited accuracy of the backward integration. Improving the backward integration would further  
 542 improve the DBFN performance and make possible the use of longer assimilation windows.

543 Our results show that the DBFN can produce results comparable to 4Dvar using lower computa-  
 544 tional power. This is because DBFN demands less iterations to converge and because one iteration  
 545 of 4Dvar corresponds to one integration of the tangent linear model, one integration of the adjoint  
 546 model, which costs four times more than one standard model integration, plus the cost of minimizing  
 547 the cost function, while the DBFN costs twice the integration of the nonlinear model.

548 The sensitivity tests show that for the 4Dvar long assimilation windows should be preferably used  
 549 because it favors the propagation of the sea surface height information to the deep layers. For the  
 550 DBFN, short windows are preferable because it reduces the effect of the diffusion-induced errors. In

551 future works it would be beneficial to account for this errors when constructing the nudging gain.

552 Finally, it appears that the DBFN algorithm is worth being further explored both on theoretical  
553 and practical aspects, especially those related to the optimization of the matrix  $\mathbf{K}$  and applications  
554 to a more realistic configuration.

555 *Acknowledgements.* This work was supported by CNRS/INSU through the LEFE/MANU program. This work  
556 was granted access to the HPC and visualization resources of "Centre de Calcul Interactif" hosted by "Université  
557 Nice Sophia Antipolis ". Calculations were also performed at the IDRIS computational facility center. The  
558 authors thanks Pierre-Antoine Bouttier for his help with the set-up of the 4Dvar algorithm.

## 559 **References**

- 560 Abarbanel, H. D. I., Kostuk, M., and Whartenby, W.: Data assimilation with regularized nonlinear instabilities,  
561 Quarterly Journal of the Royal Meteorological Society, 136, 769–783, doi:10.1002/qj.600, [http://dx.doi.org/](http://dx.doi.org/10.1002/qj.600)  
562 10.1002/qj.600, 2010.
- 563 Anderson, J. L.: A local least squares framework for ensemble filtering, Monthly Weather Review, 131, 634–  
564 642, 2003.
- 565 Anthes, R. A.: Data Assimilation and Initialization of Hurricane Prediction Models, J. Atmos.  
566 Sci., 31, 702–719, doi:10.1175/1520-0469(1974)031<0702:DAAIOH>2.0.CO;2, [http://dx.doi.org/10.1175/](http://dx.doi.org/10.1175/1520-0469(1974)031<0702:DAAIOH>2.0.CO;2)  
567 1520-0469(1974)031<0702:DAAIOH>2.0.CO;2, 1974.
- 568 Auroux, D.: The back and forth nudging algorithm applied to a shallow water model, comparison and hy-  
569 bridization with the 4D-VAR, Int. J. Numer. Methods Fluids, 61, 911–929, 2009.
- 570 Auroux, D. and Blum, J.: Back and forth nudging algorithm for data assimilation problems, C. R. Acad. Sci.  
571 Paris, Ser. I, 340, 873–878, 2005.
- 572 Auroux, D. and Blum, J.: A nudging-based data assimilation method for oceanographic problems: the Back  
573 and Forth Nudging (BFN) algorithm, Nonlin. Proc. Geophys., 15, 305–319, 2008.
- 574 Auroux, D. and Nodet, M.: The back and forth nudging algorithm for data assimilation problems: theoretical  
575 results on transport equations, ESAIM Control Optim. Calc. Var., 18, 318–342, 2012.
- 576 Auroux, D., Blum, J., and Nodet, M.: Diffusive Back and Forth Nudging algorithm for data assimilation, C. R.  
577 Acad. Sci. Paris, Ser. I, 349, 849854, 2011.
- 578 Auroux, D., Bansart, P., and Blum, J.: An evolution of the Back and Forth Nudging for geophysical data  
579 assimilation: application to Burgers equation and comparisons, Inv. Prob. Sci. Eng., 21, 399–419, 2012.
- 580 Ballabrera-Poy, J., Kalnay, E., and Yang, S.-C.: Data assimilation in a system with two scales combining two  
581 initialization techniques, Tellus A, 61, 539–549, doi:10.1111/j.1600-0870.2009.00400.x, 2009.
- 582 Bergemann, K. and Reich, S.: A mollified ensemble Kalman filter, Quarterly Journal of the Royal Meteorolog-  
583 ical Society, 136, 1636–1643, doi:10.1002/qj.672, <http://dx.doi.org/10.1002/qj.672>, 2010.
- 584 Blayo, E., Verron, J., and Molines, J.-M.: Assimilation of topex/poseidon altimeter data into a circulation model  
585 of the north atlantic., Journal of Geophysical Research: Oceans, 99, 24 691–24 705, 1994.
- 586 Blum, J., Le Dimet, F.-X., and Navon, I. M.: Data Assimilation for Geophysical Fluids, in: Computational  
587 Methods for the Atmosphere and the Oceans, edited by Ciarlet, P. G., Temam, R., and Tribbia, J., vol. 14 of  
588 *Handbook of Numerical Analysis*, pp. 385–442, Elsevier, Oxford, United Kingdom, 2008.
- 589 Bouttier, P.-A., Blayo, E., Brankart, J. M., Brasseur, P., Cosme, E., Verron, J., and Vidard, A.: Toward a data  
590 assimilation system for NEMO, Mercator Ocean Quarterly Newsletter, 46, 31–45, 2012.
- 591 Chang, K. I., Ghil, M., Ide, K., and Lai, C. C. A.: Transition to aperiodic variability in a wind-driven double-  
592 gyre circulation model., J. Phys. Oceanography, 31, 1260–1286, 2001.
- 593 Chassignet, E. P. and Gent, P. R.: The influence of Boundary Conditions on Midlatitude Jet Separation in Ocean  
594 Numerical Models., J. Phys. Oceanography, 21, 1290–1299, 1991.
- 595 Chen, X., Liu, C., ODriscoll, K., Mayer, B., Su, J., and Pohlmann, T.: On the nudging terms at open boundaries  
596 in regional ocean models, Ocean Modelling, 66, 14 – 25, doi:10.1016/j.ocemod.2013.02.006, [http://www.](http://www.sciencedirect.com/science/article/pii/S1463500313000401)  
597 [sciencedirect.com/science/article/pii/S1463500313000401](http://www.sciencedirect.com/science/article/pii/S1463500313000401), 2013.
- 598 Clifford, M., Horton, C., Schmitz, J., and Kantha, L. H.: An oceanographic nowcast/forecast system for the



599 Red Sea, *Journal of Geophysical Research: Oceans*, 102, 25 101–25 122, doi:10.1029/97JC01919, <http://dx.doi.org/10.1029/97JC01919>, 1997.

601 Cosme, E., Brankart, J.-M., Verron, J., Brasseur, P., and Krysta, M.: Implementation of a Reduced-rank, square-root smoother for ocean data assimilation, *Ocean Modelling*, 33, 87–100, 2010.

603 Courtier, P., Thepaut, J. N., and Hollingsworth, A.: A strategy for operational implementation of 4d-var, using an incremental approach., *Q. J. R. Meteorol. Soc.*, 123, 1367–1387, 1994.

605 Donovan, A., Mirrahimi, M., and Rouchon, P.: Back and forth nudging for quantum state reconstruction, in: 4th International Symposium on Communications, Control and Signal Processing, pp. 1–5, Limassol, Cyprus, 2010.

608 Evensen, G.: Sequential data assimilation with a nonlinear quasi-geostrophic model using Monte Carlo methods to forecast error statistics, *Journal of Geophysical Research: Oceans*, 99, 10 143–10 162, doi: 10.1029/94JC00572, <http://dx.doi.org/10.1029/94JC00572>, 1994.

611 Gelb, A., Kasper, J., Nash, R. A., Price, C. F., and Sutherland, A. A.: *Applied Optimal Estimation*, The M.I.T. Press, Reading, Massachusetts, arthur gelb edn., 1974.

613 Haines, K., Malanotte-Rizzoli, P., Young, R. E., and Holland, W. R.: A comparison of two methods for the assimilation of altimeter data into a shallow-water model, *Dynamics of Atmospheres and Oceans*, 17, 89 – 133, doi:10.1016/0377-0265(93)90014-X, <http://www.sciencedirect.com/science/article/pii/037702659390014X>, 1993.

617 Hunt, B. R., Kostelich, E. J., and Szunyogh, I.: Efficient data assimilation for spatiotemporal chaos: A local ensemble transform Kalman filter, *Physica D: Nonlinear Phenomena*, 230, 112 – 126, doi:10.1016/j.physd.2006.11.008, <http://www.sciencedirect.com/science/article/pii/S0167278906004647>, 2007.

620 Kalnay, E., Ki Park, S., Pu, Z., and Gao, J.: Application of the quasi-inverse method to data assimilation, *Month. Weather Rev.*, 128, 864–875, 2000.

622 Killworth, P. D., Dieterich, C., Le Provost, C., Oschlies, A., and Willebrand, J.: Assimilation of altimetric data and mean sea surface height into an eddy-permitting model of the North Atlantic, *Progress in Oceanography*, 48, 313 – 335, doi:10.1016/S0079-6611(01)00009-X, <http://www.sciencedirect.com/science/article/pii/S007966110100009X>, 2001.

626 Krysta, M., E., B., Cosme, E., and Verron, J.: A consistent hybrid variational-smoothing data assimilation method: Application to a simple shallow-water model of the turbulent mid-latitude ocean, *Month. Weath. Rev.*, 139, 3333–3347, 2011.

629 Lakshmivarahan, S. and Lewis, J.: *Nudging Methods: A Critical Overview*, in: *Data Assimilation for Atmospheric, Oceanic and Hydrologic Applications*, edited by Park, S. K. and Liang, L., vol. II, pp. 27–58, Springer Verlag, Berlin, 2012.

632 Le Dimet, F. and Talagrand, O.: Variational algorithms for analysis and assimilation of meteorological observations, *Tellus*, 38A, 97–110, 1986.

634 Leghtas, Z., Mirrahimi, M., and Rouchon, P.: Back and Forth Nudging for quantum state estimation by continuous weak measurement, in: *Proceedings of American Control Conference*, pp. 4334–4339, San Francisco, USA, 2011.

637 Lei, L., Stauffer, D., Haupt, S. E., and Young, G.: A hybrid nudging-ensemble Kalman filter approach to data assimilation. Part I: application in the Lorenz system, *Tellus A*, 64, 2012.

638

639 Leredde, Y., Devenon, J.-L., and Dekeyser, I.: Turbulent viscosity optimized by data assimilation, *Annales Geo-*  
640 *physicae*, 17, 1463–1477, doi:10.1007/s00585-999-1463-9, <http://www.ann-geophys.net/17/1463/1999/>,  
641 1999.

642 Levy, M. M., Klein, P., Trguier, A.-M., Iovino, D., Madec, G., Masson, S., and K. Takahashi, S.: Modifications  
643 of gyre circulation by sub-mesoscale physics, *Ocean Modelling*, 34, 1 – 15, doi:10.1016/j.ocemod.2010.04.  
644 001, <http://www.sciencedirect.com/science/article/pii/S1463500310000582>, 2010.

645 Lewis, J. K., Shulman, I., and Blumberg, A. F.: Assimilation of Doppler radar current data into numer-  
646 ical ocean models, *Continental Shelf Research*, 18, 541 – 559, doi:10.1016/S0278-4343(98)00006-5,  
647 <http://www.sciencedirect.com/science/article/pii/S0278434398000065>, 1998.

648 Li, H., Kanamitsu, M., and Hong, S.-Y.: California reanalysis downscaling at 10 km using an ocean-atmosphere  
649 coupled regional model system, *Journal of Geophysical Research*, doi:10.1029/2011JD017372, 2012.

650 Lingala, N., Sri Namachchivaya, N., Perkowski, N., and Yeong, H.: Optimal Nudging in Particle Filters, *Proce-*  
651 *dia {IUTAM}*, 6, 18 – 30, doi:10.1016/j.piutam.2013.01.002, [http://www.sciencedirect.com/science/article/](http://www.sciencedirect.com/science/article/pii/S2210983813000035)  
652 [pii/S2210983813000035](http://www.sciencedirect.com/science/article/pii/S2210983813000035), 2013.

653 Lions, J. L.: *Optimal Control of Systems Governed by Partial Differential Equations.*, Springer-Verlag, Berlin,  
654 Federal Replubic of Germany, first edn., 1971.

655 Luenberger, D. G.: *Observers for Multivariable Systems.*, *IEEE Transactions on Automatic Control*, 11, 190–  
656 197, doi:10.1109/TAC.1966.1098323, 1966.

657 Luo, X. and Hoteit, I.: Ensemble Kalman filtering with residual nudging, *Tellus A*, 64, doi:10.3402/tellusa.  
658 v64i0.17130, <http://www.tellusa.net/index.php/tellusa/article/view/17130>, 2012.

659 Luo, X. and Hoteit, I.: Efficient particle filtering through residual nudging, *Quarterly Journal of the Royal*  
660 *Meteorological Society*, 140, n/a–n/a, doi:10.1002/qj.2152, <http://dx.doi.org/10.1002/qj.2152>, 2013.

661 Madec, G.: *NEMO ocean engine*, Note du Pole de modlisation, Institut Pierre-Simon Laplace (IPSL), Paris,  
662 France, 27 edn., 2008.

663 Marchesiello, P., McWilliams, J. C., and Shchepetkin, A.: Open boundary conditions for long-term integration  
664 of regional oceanic models, *Ocean Modelling*, 3, 1 – 20, doi:10.1016/S1463-5003(00)00013-5, [http://www.](http://www.sciencedirect.com/science/article/pii/S1463500300000135)  
665 [sciencedirect.com/science/article/pii/S1463500300000135](http://www.sciencedirect.com/science/article/pii/S1463500300000135), 2001.

666 Mogensen, K., Balmaseda, M. A., Weaver, A. T., M., M., and Vidard, A.: NEMOVAR: A variational data  
667 assimilation system for the NEMO ocean model, *ECMWF Newsletter*, 120, 2009.

668 Molcard, A., Griffa, A., and Ozgokmen, T. M.: Lagrangian Data Assimilation in Multilayer Primitive Equation  
669 Ocean Models, *J. Atmos. and Ocean Tech.*, 22, 70–83, 2004.

670 Pham, D. T.: Stochastic methods for sequential data assimilation in strongly nonlinear systems, *Mon. Weather*  
671 *Rev.*, 129, 1494–1207, 2001.

672 Primeau, F. W.: Multiple equilibria of a double-gyre ocean model with super-slip boundary conditions., *J. Phys.*  
673 *Oceanography*, 28, 2130–2147, 1998.

674 Pu, Z., Kalnay, E., Sela, J., and Szunyogh, I.: Sensitivity of forecast errors to initial conditions with a quasi-  
675 inverse linear method, *Month. Weather Rev.*, 125, 2479–2503, 1997.

676 Ramdani, K., Tucsna, M., and Weiss, G.: Recovering the initial state of an infinite-dimensional system using  
677 observer, *Automatica*, 2010.

678 Roullet, G. and Madec, G.: salt conservation, free surface, and varying levels : a new formulation for ocean

679 general circulation models., *J. Geophys. Res.*, 105, 23,927–23,942, 2000.

680 Skamarock, W. C.: Evaluating Mesoscale NWP Models Using Kinetic Energy Spectra, *Mon. Wea. Rev.*, 132,  
681 3019–3032, 2004.

682 Stauffer, D. and Bao, J.-W.: Optimal determination of nudging coefficients using the adjoint equations, *Tellus*  
683 *A*, 45, 358–369, 1993.

684 Tenenhaus, M.: *La régression PLS : Théorie et Pratique.*, éditions Technip, Paris, France, first edn., 1998.

685 Thompson, K. R., Wright, D. G., Lu, Y., and Demirov, E.: A simple method for reducing seasonal bias and  
686 drift in eddy resolving ocean models, *Ocean Modelling*, 13, 109 – 125, doi:10.1016/j.ocemod.2005.11.003,  
687 <http://www.sciencedirect.com/science/article/pii/S1463500305000910>, 2006.

688 Verron, J.: Nudging satellite altimeter data into quasi-geostrophic ocean models, *Journal of Geophysical Re-*  
689 *search: Oceans*, 97, 7479–7491, doi:10.1029/92JC00200, <http://dx.doi.org/10.1029/92JC00200>, 1992.

690 Vidard, P. A., Le Dimet, F.-X., and Piacentini, A.: Determination of optimal nudging coefficients, *Tellus A*,  
691 55, 1–15, doi:10.1034/j.1600-0870.2003.201317.x, <http://dx.doi.org/10.1034/j.1600-0870.2003.201317.x>,  
692 2003.

693 Wang, K., Debernard, J., Sperrevik, A. K., Isachsen, E., and Lavergne, T.: A combined optimal interpolation  
694 and nudging scheme to assimilate OSISAF sea-ice concentration into ROMS, *Annals of Glaciology*, 54,  
695 8–12, 2013.

696 Weaver, A. and Courtier, P.: Correlation modelling on the sphere using a generalized diffusion equation,  
697 *Quarterly Journal of the Royal Meteorological Society*, 127, 1815–1846, doi:10.1002/qj.49712757518,  
698 <http://dx.doi.org/10.1002/qj.49712757518>, 2001.

699 Weaver, A. T., Deltel, C., Machu, E., Ricci, S., and Daget, N.: A multivariate balance operator for variational  
700 ocean data assimilation, *Q. J. R. Meteorol. Soc.*, 131, 3605–3625, 2005.

701 Willians, P. D.: A Proposed Modification to the Robert Asselin Time Filter., *Month. Weather Rev.*, 137, 2538–  
702 2546, 2009.

703 Zou, X., Navon, I. M., and Le Dimet, F. X.: An Optimal Nudging Data Assimilation Scheme Using Param-  
704 eter Estimation, *Quarterly Journal of the Royal Meteorological Society*, 118, 1163–1186, doi:10.1002/qj.  
705 49711850808, <http://dx.doi.org/10.1002/qj.49711850808>, 1992.